Numer. Math. Theor. Meth. Appl. Vol. **3**, No. 1, pp. 53-78
doi: 10.4208/nmtma.2009.m9006 February 2010

A Modified Polynomial Preserving Recovery and Its Applications to A Posteriori Error Estimates

Haijun Wu*

Department of Mathematics, Nanjing University, Jiangsu, 210093, China.

Received 11 April 2009; Accepted (in revised version) 28 April 2009

Available online 30 November 2009

Abstract. A modified polynomial preserving gradient recovery technique is proposed. Unlike the polynomial preserving gradient recovery technique, the gradient recovered with the modified polynomial preserving recovery (MPPR) is constructed element-wise, and it is discontinuous across the interior edges. One advantage of the MPPR technique is that the implementation is easier when adaptive meshes are involved. Superconvergence results of the gradient recovered with MPPR are proved for finite element methods for elliptic boundary problems and eigenvalue problems under adaptive meshes. The MPPR is applied to adaptive finite element methods to construct asymptotic exact a posteriori error estimates. Numerical tests are provided to examine the theoretical results and the effectiveness of the adaptive finite element algorithms.

AMS subject classifications: 65N30, 65N15, 45K20

Key words: Adaptive finite element method, superconvergence, gradient recovery, modified PPR.

1. Introduction

Gradient recovery has been widely used for a posteriori error estimates (see, e.g., [1, 4, 9, 12, 20, 21, 25, 26, 32, 34–37]). Comparing with the a posteriori error estimates of residual type (see, e.g., [1,2,7,10,16,17,22,24]), the a posteriori error estimates based on gradient recovery have the advantages of problem-independence and asymptotic exactness. Although the effectiveness of using the a posteriori error estimates based on gradient recovery in adaptive finite element methods have been demonstrated by many practical applications, most theoretical results assume uniform meshes and sufficiently smooth solutions (see, e.g., [5,8,14,15,18,27,28,30,31,33]). Recently, Wu and Zhang [25] consider adaptive finite element methods for elliptic problems with domain corner singularities and prove a superconvergence result for recovered gradient by the polynomial preserving recovery (PPR) as well as the asymptotic exactness of the a posteriori error estimate based on PPR under two mesh conditions. One condition is similar to but weaker than the *Condition* (α,σ) used for uniform meshes (cf. [18,27,30,31]). Another one is a mesh density

*Corresponding author. *Email address:* `hjw@nju.edu.cn` (H. Wu)

condition. The two conditions are verified numerically by real-life adaptive meshes (see, e.g., [25,26]). The results in [25] have been applied to enhance the eigenvalue approximations by the finite element method (see [26]).

Let $\Omega \subset \mathbb{R}^2$ be a bounded polygonal domain with boundary $\partial\Omega$. Let $\mathscr{M}_h$ be a regular triangulation of Ω, $\mathscr{E}_h$ be the set of all interior edges, and $\mathscr{N}_h$ be the set of all nodal points. Assume that the origin $O \in \mathscr{N}_h$ and any triangle $\tau \in \mathscr{M}_h$ is considered as closed. Let $V_h^k = \left\{v_h : v_h \in H^1(\Omega), v_h|_\tau \in P_k(\tau), \forall \tau \mathscr{M}_h\right\}$ be the conforming finite element space associated with $\mathscr{M}_h$. Here P_k denotes the set of polynomials with degree $\leq k$. We remark that we will use the total degrees of freedom N (instead of the maximum mesh size h) to measure the rate of convergence. However, for notational convenience, we are still using h as an index.

Given a continuous function φ, the recovered gradient by PPR, $G_h\varphi$, is a vector function in $V_h^k \times V_h^k$ that is defined as follows [18,19]. For a node $z \in \mathscr{N}_h$, we select $n \geq (k+2)(k+3)/2$ sampling points $z_j \in \mathscr{N}_h$, $j = 1, 2, \cdots, n$, in an element patch ω_z containing z (z is one of z_j), and fit a polynomial of degree $k+1$, in the least squares sense, with values of φ at those sampling points. In other words, we are looking for $p_{k+1} \in \mathscr{P}_{k+1}$ such that

$$\sum_{j=1}^{n}(p_{k+1} - \varphi)^2(z_j) = \min_{q \in \mathscr{P}_{k+1}} \sum_{j=1}^{n}(q - \varphi)^2(z_j). \tag{1.1}$$

The recovered gradient at z is then defined as

$$G_h\varphi(z) = (\nabla p_{k+1})(z). \tag{1.2}$$

Suppose u is an unknown solution and $u_h \in V_h^k$ is an approximation of u. If $G_h u_h$ is a better approximation than ∇u_h, then we can use $\left\|G_h u_h - \nabla u_h\right\|$ as an a posteriori error estimate of $\left\|\nabla u - \nabla u_h\right\|$.

Note that the recovered gradient by PPR is constructed node-wise. In the case of adaptive refined meshes, the number of elements surround a node may varies for different nodes. This makes the implementation of PPR on adaptive meshes a little complicated, in particular dealing with the boundary nodes. Inspiring by the fact that the local a posteriori indicators are usually calculated element-wise, we introduce a modified polynomial preserving gradient recovery which is construct element-wise. That is, for any element $\tau \in \mathscr{M}_h$, we choose sampling points from the nodes in an element patch ω_τ containing τ and construct recovered gradient on τ. For interior element τ, the element patch ω_τ can be chosen as the union of τ and the three elements that have common edges with τ. Note that ω_τ has the same topology structure for interior elements. We refer to Fig. 1 for some possible choices of sampling points. For an element τ whose one edge is on the boundary of Ω, a simple choice of ω_τ is $\omega_{\tau'}$, where τ' is an interior element that has a common edge with the element τ.

In this paper, we extend the results in [25] and [26] on PPR to the case of the modified polynomial preserving recovery (MPPR). We first consider the application of recovered gradient by MPPR to adaptive finite element methods for elliptic problems. The superconvergence of the recovered gradient by MPPR and the exactness of the a posteriori error estimate based on MPPR are proved for the Poisson's equation under the two mesh conditions

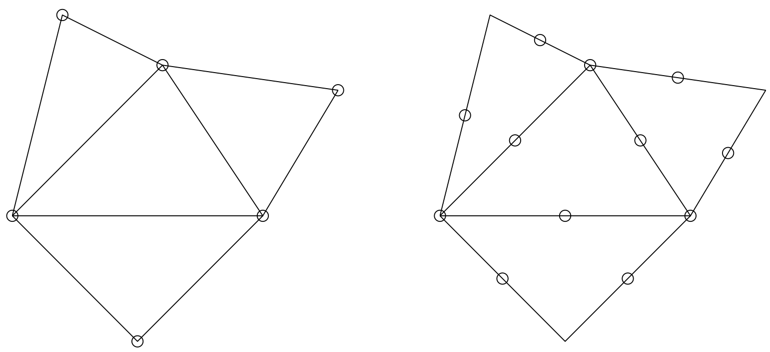

Figure 1: Possible choices of sampling points for an interior triangle τ for the linear (left) and quadratic (right) elements.

introduced in [25]. By shifting the error estimator in the standard residual based adaptive finite element method from residual based to recovery based, we have obtained the same numerical convergence rate following the same mark-up and refinement procedure for two model problems – the Poisson's equation on the cracked square and a checkerboard problem with discontinuous coefficient. We demonstrate that the meshes produced by the standard adaptive procedure in both of our model problems indeed satisfy the two mesh conditions. Superconvergences of the recovered gradients by MPPR are observed for both of our model problems, although our current theoretical results do not cover the case of discontinuous coefficients.

Secondly we consider the application of recovered gradient by MPPR to adaptive finite element methods for finding eigenvalues of the Laplace operator. Let (λ_j, u_j) be the j-th eigenpair and let (λ_{jh}, u_{jh}) be its finite element approximation. Denote by $\widehat{G}_h u_{jh}$ the recovered gradient by MPPR from u_{jh}. It is proved that $\left\|\widehat{G}_h u_{jh} - \nabla u_{jh}\right\|^2_{L^2(\Omega)}$is an asymptotic exact a posteriori error estimative for $\lambda_{jh} - \lambda_j$ and therefore

$$\lambda^*_{jh} = \lambda_{jh} - \left\|\widehat{G}_h u_{jh} - \nabla u_{jh}\right\|^2_{L^2(\Omega)}$$

is a better approximation than λ_{jh}. The theoretical results are verified numerically by an eigenvalue problem on the cracked disk. The effect of choosing different discrete eigenfunctions in the a posteriori error estimates on the errors of discrete eigenvalues is also discussed. Upon the numerical tests, we suggest to use the a posteriori error estimates based on the j-th discrete eigenfunctions if only the j-th eigenvalue is cared, and to use the a posteriori error estimates based on the 1-st discrete eigenfunctions if the first ℓ eigenvalues are all needed, where ℓ is a positive integer.

Throughout the paper, we use the notation $A \lesssim B$ to represent the inequality $A \leq constant \times B$, where the *constant* depends only on the minimum angle of the triangles in $\mathscr{M}_h$, the domain Ω, and the constant δ that characterizes the singularity of the solution (see (2.1) and (2.2)). The notation $A \approx B$ is equivalent to $A \lesssim B$ and $B \lesssim A$.

The layout of the paper is as follows. In Section 2, we recall the two mesh conditions introduced in [25] and a superconvergence result on the PPR operator. The MPPR operator is introduced in Section 3. Superconvergence results of the recovered gradient by MPPR are established. We discuss the applications of recovered gradient by MPPR to the a posteriori error estimates for finite element methods for elliptic problems in Section 4 and for eigenvalue problems in Section 5.

2. Preliminary

In this section we recall the two mesh conditions introduced in [25] and some superconvergence results.

Suppose the origin O is a vertex of Ω. In this paper we are interested in the function u that has a singularity at the origin O and can be decomposed as a sum of a singular part and a smooth part:

$$u = v + w, \tag{2.1}$$

where

$$\left|\frac{\partial^m v}{\partial x^i \partial y^{m-i}}\right| \lesssim r^{\delta-m} \quad \text{and} \quad \left|\frac{\partial^m w}{\partial x^i \partial y^{m-i}}\right| \lesssim 1, \quad m = 1, \cdots, k+2, \ \ i = 0, \cdots, m. \tag{2.2}$$

Here $r = \sqrt{x^2 + y^2}$ and $0 < \delta < k + 1$ is a constant. Here $k = 1$ for linear finite element and $k = 2$ for quadratic finite element.

We remark that the solutions of the elliptic problems and eigenfunctions of the eigenvalue problems considered in this paper do have decompositions as above (see, e.g., [11, 25, 26]).

2.1. Mesh quality

We first introduce some notation (See Fig. 2). For an edge $e \in \mathscr{E}_h$, which is shared by two elements τ and τ', let $\Omega_e = \tau \cup \tau'$ be the patch of e, h_e denote the length of e, and r_e be the distance from the origin O to the midpoint of e. For any $\tau \in \mathscr{M}_h$, we denote by h_τ its diameter and by r_τ the distance from the origin to the barycenter of τ.

Given an interior edge $e \in \mathscr{E}_h$, we say that Ω_e is an ε approximate parallelogram if the lengths of any two opposite edges differ only by ε.

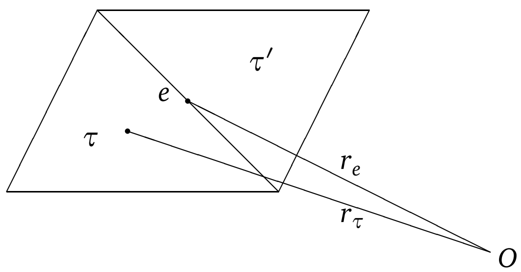

Figure 2: Notation in the patch Ω_e.

Definition 2.1. *A family of triangulations $\{\mathscr{M}_h\}$ is said to satisfy Condition (α,σ,μ) if there exist constants $\alpha>0, 0\le\sigma<1$, and $\mu>0$ such that the interior edges can be separated into two parts $\mathscr{E}_h=\mathscr{E}_{1,h}\oplus\mathscr{E}_{2,h}$: Ω_e forms an ε_e parallelogram with $\varepsilon_e\lesssim h_e^{1+\alpha}/r_e^{\alpha+\mu(1-\alpha)}$ for $e\in\mathscr{E}_{1,h}$ and the number of edges in $\mathscr{E}_{2,h}$ satisfies $\#\mathscr{E}_{2,h}\lesssim N^{\sigma}$.*

Remark 2.1. The meaning of *Condition* (α,σ,μ) is the following. The edges can be grouped into "good" ($\mathscr{E}_{1,h}$) and "bad" ($\mathscr{E}_{2,h}$), where the number of bad edges are much smaller than that of good edges. The ratio is

$$\frac{\#\mathscr{E}_{2,h}}{\#\mathscr{E}_{1,h}}\lesssim\frac{N^{\sigma}}{N}=\frac{1}{N^{1-\sigma}}.$$

When $r_e=\mathscr{O}(1)$, i.e., an edge e is far away from the singular point O, more restrictions are put on the triangle pair with the common edge e. The mesh condition requires that the two triangles form an $\mathscr{O}(h_e^{1+\alpha})$ parallelogram, which is the same as in previous works (see, e.g., [18–20, 27]). When e is in a neighborhood of O, if $h_e\eqsim r_e^{1+\mu(1-\alpha)/\alpha}$, then the condition (α,σ,μ) is fulfilled by those edges such that Ω_e is an $\mathscr{O}(h_e)$ parallelogram, which means no restriction at all. Roughly speaking, number of edges in $\mathscr{E}_{1,h}$ that have no restriction imposed is $\mathscr{O}(N^{1-\alpha})$ if $h_\tau\eqsim r_\tau^{1-\mu}\underline{h}^{\mu}$ for any $\tau\in\mathscr{M}_h$. Here $\underline{h}$ and μ are positive constants. An explanation is given in [25].

We see from the above discussion that, the closer to the singular point, the less restriction is imposed on the mesh. As a matter of fact, for an adaptively refined mesh, the closer to the singular point, the worse the mesh quality is, in the sense of forming parallelograms.

In Section 4, we demonstrate that the aforementioned mesh condition is satisfied by actual adaptive meshes on two benchmark problems: the elliptic problem on a domain with a crack and the checkerboard problem.

The following lemma provides an estimate for the total degrees of freedom N when the mesh $\mathscr{M}_h$ satisfies $h_\tau\eqsim r_\tau^{1-\mu}\underline{h}^{\mu}$. The proof can be found in [25].

Lemma 2.1. *Assume that $h_\tau\eqsim r_\tau^{1-\mu}\underline{h}^{\mu}$ for any $\tau\in\mathscr{M}_h$, where $\underline{h}$ and μ are positive constants. Then the degrees of freedom N of the finite element space V_h^k satisfies*

$$N\eqsim\frac{1}{\underline{h}^{2\mu}}. \tag{2.3}$$

Remark 2.2. The condition $h_\tau\eqsim r_\tau^{1-\mu}\underline{h}^{\mu}$ can be viewed as a discrete mesh density function. The positive number $\underline{h}\eqsim\min_{\tau\in\mathscr{M}_h}h_\tau$ is the size of the minimum element. For an element τ in the neighborhood of O, we have $r_\tau\eqsim h_\tau$ and the condition $h_\tau\eqsim r_\tau^{1-\mu}\underline{h}^{\mu}$ implies $h_\tau\eqsim\underline{h}$. Roughly speaking, the condition $h_\tau\eqsim r_\tau^{1-\mu}\underline{h}^{\mu}$ indicates that the triangles in $\mathscr{M}_h$ are distributed according to the circles with radiuses $m^{1/\mu}\underline{h}$ and common center the origin, $m=1,2,3,\cdots$. In the rest of the paper, we choose $\mu=\delta/2$ for linear element and $\mu=\delta/3$ for quadratic element.

2.2. Superconvergence between the elliptic projection and the finite element interpolation

Let $I_h : C(\Omega) \mapsto V_h^k$ be the standard Lagrange interpolation operator. Define $\overset{\circ}{V}{}_h^k = V_h^k \bigcap H_0^1(\Omega)$. We further introduce the elliptic projector $P_h : H^1(\Omega) \mapsto V_h^k$ such that $P_h\phi = I_h\phi$ on $\partial\Omega$ and

$$\int_\Omega \nabla\phi \cdot \nabla v_h = \int_\Omega \nabla P_h\phi \cdot \nabla v_h, \quad \forall v_h \in \overset{\circ}{V}{}_h^k. \tag{2.4}$$

The following superconvergence of $\left\|\nabla I_h u - \nabla P_h u\right\|_{L^2(\Omega)}$ is proved in [25, Theorems 3.4 and 4.5].

Theorem 2.1. *Suppose* $k = 1, 2$. *Assume that* u *satisfies* (2.1)-(2.2). *Assume that* $\mathcal{M}_h$ *satisfies Condition* $(\alpha, \sigma, \delta/(k+1))$ *with* $0 < \alpha \le 1$ *and* $0 \le \sigma < 1$, *and that* $h_\tau \approx r_\tau^{1-\delta/(k+1)} \underline{h}^{\delta/(k+1)}$ *for any* $\tau \in \mathcal{M}_h$. *Then*

$$\left\|\nabla I_h u - \nabla P_h u\right\|_{L^2(\Omega)} \lesssim \frac{1 + (\ln N)^{1/2}}{N^{k/2+\rho}}, \quad \rho = \min\left(\frac{\alpha}{2}, \frac{1-\sigma}{2}\right). \tag{2.5}$$

2.3. The PPR operator G_h

Recall that G_h is defined by (1.1) and (1.2). Let u satisfy (2.1)-(2.2). Under the assumptions of Theorem 2.1, the following superconvergence of the gradient recovery of u from its elliptic projection is proved in [25, Theorems 5.3 and 5.5]:

$$\left\|G_h P_h u - \nabla u\right\|_{L^2(\Omega)} \lesssim \frac{1 + (\ln N)^{1/2}}{N^{k/2+\rho}}, \quad \rho = \min\left(\frac{\alpha}{2}, \frac{1-\sigma}{2}\right). \tag{2.6}$$

3. The modified polynomial preserving recovery operator

In this section, we first introduce an abstract framework for superconvergent gradient recovery. Then introduce the modified PPR operator $\widehat{G}_h$ that satisfies the framework.

3.1. An abstract framework

Recall that the above PPR operator is onto $V_h^k \times V_h^k$ and is defined node-wise. The definition of the modified PPR operator $\widehat{G}_h$ is similar except it is defined element-wise and is onto $\widehat{V}_h^k \times \widehat{V}_h^k$ where

$$\widehat{V}_h^k = \left\{v_h : \ v_h|_\tau \in P_k(\tau), \ \forall \tau \in \mathcal{M}_h\right\}$$

is the space of discontinuous piecewise polynomials of degree $\le k$. In this subsection, we first provide conditions for $\widehat{G}_h$ under which superconvergence estimates may be derived. The concrete definition of $\widehat{G}_h$ that satisfies the conditions will be given later. For any element $\tau \in \mathcal{M}_h$, choose an element patch ω_τ containing τ. Assume $\widehat{G}_h : C(\Omega) \mapsto \widehat{V}_h^k \times \widehat{V}_h^k$ is a linear operator that satisfies the following two conditions:

(i) For any element τ, $\widehat{G}_h p\big|_\tau = \nabla p\big|_\tau$ if $p\big|_{\omega_\tau} \in P_{k+1}(\omega_\tau)$;

(ii) $\left|(\widehat{G}_h \phi)(z)\right| \lesssim \frac{1}{h_\tau} \max_{z' \in \mathcal{N}_h \cap \omega_\tau} \left|\phi(z')\right|$ for any node z in an element $\tau \in \mathcal{M}_h$.

The following lemma gives a stability estimate and an approximation estimate of the modified PPR operator $\widehat{G}_h$.

Lemma 3.1. *Under conditions* (i) *and* (ii)*, the operator $\widehat{G}_h$ satisfies*

$$\left\|\widehat{G}_h v_h\right\|_{L^2(\Omega)} \lesssim \left\|\nabla v_h\right\|_{L^2(\Omega)}, \quad \forall v_h \in V_h^k. \tag{3.1}$$

Moreover, for any element $\tau \in \mathcal{M}_h$ and any function $\phi \in W^{k+2,\infty}(\omega_\tau)$,

$$\left\|\widehat{G}_h I_h \phi - \nabla \phi\right\|_{L^2(\tau)} \lesssim h_\tau^{k+2} \left|\phi\right|_{W^{k+2,\infty}(\omega_\tau)}, \tag{3.2}$$

where $I_h\phi$ is the finite element interpolant of ϕ onto V_h^k.

Proof. From (i), it is clear that $\widehat{G}_h C = 0$ for any constant C. From (ii), for any constants c_τ with $\tau \in \mathcal{M}_h$,

$$\begin{aligned} \left\|\widehat{G}_h v_h\right\|_{L^2(\Omega)}^2 &= \sum_{\tau \in \mathcal{M}_h} \left\|\widehat{G}_h (v_h - c_\tau)\right\|_{L^2(\tau)}^2 \lesssim \sum_{\tau \in \mathcal{M}_h} \sum_{z \in \mathcal{N}_h \cap \tau} h_\tau^2 \left|\widehat{G}_h (v_h - c_\tau)(z)\right|^2 \\ &\lesssim \sum_{\tau \in \mathcal{M}_h} \max_{z' \in \mathcal{N}_h \cap \omega_\tau} \left|v_h(z') - c_\tau\right|^2 \lesssim \sum_{\tau \in \mathcal{M}_h} h_\tau^{-2} \left\|v_h - c_\tau\right\|_{L^2(\omega_\tau)}^2. \end{aligned}$$

Then (3.1) follows from the Bramble-Hilbert lemma.

Next we prove (3.2). Let $I_h \nabla \phi$ be the interpolant of $\nabla \phi$. Then

$$\left\|\widehat{G}_h I_h \phi - \nabla \phi\right\|_{L^2(\tau)} \le \left\|\widehat{G}_h I_h \phi - I_h \nabla \phi\right\|_{L^2(\tau)} + \left\|I_h \nabla \phi - \nabla \phi\right\|_{L^2(\tau)}. \tag{3.3}$$

The standard theory of finite element interpolation estimates ([6]) says that

$$\left\|I_h \nabla \phi - \nabla \phi\right\|_{L^2(\tau)} \lesssim h_\tau^{k+1} \left|\phi\right|_{H^{k+2}(\tau)} \lesssim h_\tau^{k+2} \left|\phi\right|_{W^{k+2,\infty}(\omega_\tau)}. \tag{3.4}$$

For a node $z \in \tau$, let $\phi_{k+1}(x,y)$ be the $(k+1)$-th Taylor polynomial of ϕ at the point z. It is clear that

$$\left|\phi(x,y) - \phi_{k+1}(x,y)\right| \lesssim h_\tau^{k+2} \left|\phi\right|_{W^{k+2,\infty}(\omega_\tau)}, \quad \forall (x,y) \in \omega_\tau.$$

By conditions (i) and (ii),

$$\begin{aligned} \left|\left(\widehat{G}_h I_h \phi - I_h \nabla \phi\right)(z)\right| &= \left|\left(\widehat{G}_h I_h \phi - \nabla \phi\right)(z)\right| = \left|\left(\widehat{G}_h (I_h \phi - \phi_{k+1}) - (\nabla \phi - \nabla \phi_{k+1})\right)(z)\right| \\ &= \left|\left(\widehat{G}_h (I_h \phi - \phi_{k+1})\right)(z)\right| \lesssim \frac{1}{h_\tau} \max_{z' \in \mathcal{N}_h \cap \omega_\tau} \left|(\phi - \phi_{k+1})(z')\right| \\ &\lesssim h_\tau^{k+1} \left|\phi\right|_{W^{k+2,\infty}(\omega_\tau)}. \end{aligned}$$

Therefore

$$\left\|\widehat{G}_h I_h \phi - I_h \nabla \phi\right\|_{L^2(\tau)} \lesssim h_\tau \max_{z \in \mathcal{N}_h \cap \tau} \left|\left(\widehat{G}_h I_h \phi - I_h \nabla \phi\right)(z)\right| \lesssim h_\tau^{k+2} \left|\phi\right|_{W^{k+2,\infty}(\omega_\tau)}. \tag{3.5}$$

Combining (3.3)-(3.5) gives (3.2). This completes the proof of the lemma. □

The following theorem is devoted to the estimate of $\left\|\widehat{G}_h I_h u - \nabla u\right\|_{L^2(\Omega)}$.

Theorem 3.1. *Assume that u satisfies* (2.1)-(2.2) *and that $h_\tau \approx r_\tau^{1-\delta/(k+1)} \underline{h}^{\delta/(k+1)}$ for any $\tau \in \mathscr{M}_h$. Then, under conditions* (i) *and* (ii),

$$\left\| \widehat{G}_h I_h u - \nabla u \right\|_{L^2(\Omega)} \lesssim \frac{1 + (\ln N)^{1/2}}{N^{(k+1)/2}}. \tag{3.6}$$

Proof. Recall the decomposition $u = v + w$. We have

$$\left\| \widehat{G}_h I_h u - \nabla u \right\|_{L^2(\Omega)} \le \left\| \widehat{G}_h I_h v - \nabla v \right\|_{L^2(\Omega)} + \left\| \widehat{G}_h I_h w - \nabla w \right\|_{L^2(\Omega)}. \tag{3.7}$$

We first estimate the singular part $\left\| \widehat{G}_h I_h v - \nabla v \right\|_{L^2(\Omega)}$. Introduce the set of triangles $\mathscr{M}^O = \{\tau \in \mathscr{M}_h : \text{ the origin } O \in \omega_\tau\}$. For any $\tau \in \mathscr{M}^O$,

$$\left\| \widehat{G}_h I_h v - \nabla v \right\|_{L^2(\tau)} \le \left\| \widehat{G}_h I_h v \right\|_{L^2(\tau)} + \|\nabla v\|_{L^2(\tau)}. \tag{3.8}$$

From (i) and (ii),

$$\begin{aligned}
\left\| \widehat{G}_h I_h v \right\|_{L^2(\tau)} &= \left\| \widehat{G}_h (I_h v - v(O)) \right\|_{L^2(\tau)} \lesssim h_\tau \max_{z \in \mathscr{N}_h \cap \tau} \left| \widehat{G}_h \big(I_h v - v(O)\big)(z) \right| \\
&\lesssim h_\tau \frac{1}{h_\tau} \max_{z' \in \mathscr{N}_h \cap \omega_\tau} \left| v(z') - v(O) \right| \\
&= \max_{z' \in \mathscr{N}_h \cap \omega_\tau} \left| \int_0^1 \frac{d}{dt} v(z' t) \mathrm{d}t \right| = \max_{z' \in \mathscr{N}_h \cap \omega_\tau} \left| \int_0^1 z' \cdot \nabla v(z' t) \mathrm{d}t \right|.
\end{aligned}$$

Since $\tau \in \mathscr{M}^O$, $\left| z' \right| \lesssim \underline{h}$. It follows from the assumption (2.2) that

$$\left\| \widehat{G}_h I_h v \right\|_{L^2(\tau)} \lesssim \int_0^1 \underline{h}^\delta \cdot t^{\delta - 1} \mathrm{d}t \lesssim \underline{h}^\delta. \tag{3.9}$$

On the other hand,

$$\|\nabla v\|_{L^2(\tau)} \lesssim \Big(\int_\tau |\nabla v|^2 \Big)^{1/2} \lesssim \Big(\int_\tau r^{2\delta - 2} \Big)^{1/2} \lesssim \Big(\int_0^{c\underline{h}} r^{2\delta - 2} r \, \mathrm{d}r \Big)^{1/2} \lesssim \underline{h}^\delta. \tag{3.10}$$

Here $c\underline{h}$ is the diameter of ω_τ. Combining (3.8), (3.9), and (3.10), we obtain

$$\left\| \widehat{G}_h I_h v - \nabla v \right\|_{L^2(\tau)} \lesssim \underline{h}^\delta, \quad \text{for } \tau \in \mathscr{M}^O. \tag{3.11}$$

It follows from Lemma 3.1 and (2.2) that

$$\left\| \widehat{G}_h I_h v - \nabla v \right\|_{L^2(\tau)} \lesssim h_\tau^{k+2} |v|_{W^{k+2,\infty}(\omega_\tau)} \lesssim h_\tau^{k+2} r_\tau^{\delta - k - 2}, \quad \text{for } \tau \in \mathscr{M}_h \setminus \mathscr{M}^O, \tag{3.12}$$

where r_τ is the distance form O to the barycenter of τ. From (3.11), (3.12), and the assumption $h_\tau \approx r_\tau^{1-\delta/(k+1)} \underline{h}^{\delta/(k+1)}$,

$$
\begin{aligned}
&\left\|\widehat{G}_h I_h v - \nabla v\right\|_{L^2(\Omega)}^2 \\
&= \sum_{\tau\in\mathscr{M}_h} \left\|\widehat{G}_h I_h v - \nabla v\right\|_{L^2(\tau)}^2 \lesssim \underline{h}^{2\delta} + \sum_{\tau\in\mathscr{M}_h\backslash\mathscr{M}^O} h_\tau^{2k+4} r_\tau^{2\delta-2k-4} \\
&\lesssim \underline{h}^{2\delta} + \sum_{\tau\in\mathscr{M}_h\backslash\mathscr{M}^O} h_\tau^2 r_\tau^{2k+2-2\delta} \underline{h}^{2\delta} r_\tau^{2\delta-2k-4} \lesssim \underline{h}^{2\delta} + \sum_{\tau\in\mathscr{M}_h\backslash\mathscr{M}^O} \underline{h}^{2\delta} h_\tau^2 r_\tau^{-2} \\
&\lesssim \underline{h}^{2\delta} + \underline{h}^{2\delta} \sum_{\tau\in\mathscr{M}_h\backslash\mathscr{M}^O} \int_\tau r^{-2} \lesssim \underline{h}^{2\delta} + \underline{h}^{2\delta} \int_{\underline{h}}^1 r^{-1}\,\mathrm{d}r \lesssim \underline{h}^{2\delta} + \underline{h}^{2\delta}\left|\ln \underline{h}\right|.
\end{aligned}
$$

Therefore Lemma 2.1 implies that

$$
\left\|\widehat{G}_h I_h v - \nabla v\right\|_{L^2(\Omega)} \lesssim \underline{h}^{\delta}\left(1 + \left|\ln \underline{h}\right|^{1/2}\right) \lesssim \frac{1 + (\ln N)^{1/2}}{N^{(k+1)/2}}. \tag{3.13}
$$

Next we turn to estimate the term $\left\|\widehat{G}_h I_h w - \nabla w\right\|_{L^2(\Omega)}$ in (3.7). Since w is smooth, we do not have to divide $\mathscr{M}_h$ into two parts as above. From Lemma 3.1 and the assumption (2.2),

$$
\begin{aligned}
\left\|\widehat{G}_h I_h w - \nabla w\right\|_{L^2(\Omega)} &\lesssim \Big(\sum_{\tau\in\mathscr{M}_h} \left\|\widehat{G}_h I_h w - \nabla w\right\|_{L^2(\tau)}^2\Big)^{1/2} \lesssim \Big(\sum_{\tau\in\mathscr{M}_h} h_\tau^{2k+4}\Big)^{1/2} \\
&\lesssim \Big(\sum_{\tau\in\mathscr{M}_h} h_\tau^2 r_\tau^{2k+2-2\delta} \underline{h}^{2\delta}\Big)^{1/2} \lesssim \underline{h}^{\delta}\Big(\int_\Omega r^{2k+2-2\delta}\Big)^{1/2} \\
&\lesssim \underline{h}^{\delta} \lesssim \frac{1}{N^{(k+1)/2}}.
\end{aligned} \tag{3.14}
$$

The proof of the theorem is completed by inserting the estimates (3.13) and (3.14) into the inequality (3.7). □

We next consider the superconvergence estimate for $\left\|\widehat{G}_h P_h u - \nabla u\right\|_{L^2(\Omega)}$, where the elliptic projector P_h is defined in (2.4). We have from Lemma 3.1,

$$
\begin{aligned}
\left\|\widehat{G}_h P_h u - \nabla u\right\|_{L^2(\Omega)} &\le \left\|\widehat{G}_h P_h u - \widehat{G}_h I_h u\right\|_{L^2(\Omega)} + \left\|\widehat{G}_h I_h u - \nabla u\right\|_{L^2(\Omega)} \\
&\lesssim \left\|\nabla(P_h u - I_h u)\right\|_{L^2(\Omega)} + \left\|\widehat{G}_h I_h u - \nabla u\right\|_{L^2(\Omega)}.
\end{aligned} \tag{3.15}
$$

Here $I_h u$ is the finite element interpolant of u. The following superconvergence result for the gradient recovery operator $\widehat{G}_h$ may be proved by combining (3.15), Theorem 2.1, and Theorem 3.1.

Theorem 3.2. *Suppose $k = 1, 2$. Assume that u satisfies* (2.1)-(2.2). *Assume that $\mathscr{M}_h$ satisfies Condition $(\alpha, \sigma, \delta/(k+1))$ with $0 < \alpha \le 1$ and $0 \le \sigma < 1$, and that $h_\tau \approx r_\tau^{1-\delta/(k+1)} \underline{h}^{\delta/(k+1)}$ for any $\tau \in \mathscr{M}_h$. Then, under conditions* (i) *and* (ii),

$$
\left\|\widehat{G}_h P_h u - \nabla u\right\|_{L^2(\Omega)} \lesssim \frac{1 + (\ln N)^{1/2}}{N^{k/2+\rho}}, \quad \rho = \min\Big(\frac{\alpha}{2}, \frac{1-\sigma}{2}\Big). \tag{3.16}
$$

We remark that the result of Theorem 3.2 is a superconvergence result since the asymptotically optimal convergence rate of $\left\|\nabla(u-P_hu)\right\|_{L^2(\Omega)}$ is $\mathscr{O}(1/N^{k/2})$ (see the following lemma).

Lemma 3.2. *Let u satisfy* (2.1)-(2.2). *Assume that $h_\tau \eqsim r_\tau^{1-\delta/(k+1)}\underline{h}^{\delta/(k+1)}$ for any $\tau\in\mathscr{M}_h$. Then*

$$\left\|\nabla(u-I_hu)\right\|_{L^2(\Omega)} \lesssim \frac{1}{N^{k/2}} \quad \text{and hence} \quad \left\|\nabla(u-P_hu)\right\|_{L^2(\Omega)} \lesssim \frac{1}{N^{k/2}}.$$

Proof. Let $\mathscr{M}^{\widetilde{O}}=\{\tau\in\mathscr{M}_h: \text{ the origin } O\in\partial\tau\}$ be the set of elements with one vertex at O. Recall that u is decomposed as $u=v+w$ satisfying (2.2). For any $\tau\in\mathscr{M}^{\widetilde{O}}$,

$$\left\|\nabla v-\nabla I_hv\right\|_{L^2(\tau)} \lesssim \left\|\nabla v\right\|_{L^2(\tau)}+\left\|\nabla I_hv\right\|_{L^2(\tau)}.$$

Since $\nabla C=0$, for any constant C, by a similar argument to that for (3.11) (see also [25, Lemma3.2]), we have,

$$\left\|\nabla v-\nabla I_hv\right\|_{L^2(\tau)} \lesssim h_\tau^\delta, \quad \forall\tau\in\mathscr{M}^{\widetilde{O}}. \tag{3.17}$$

Noticing that

$$\left\|\nabla(v-I_hv)\right\|_{L^2(\tau)} \lesssim h_\tau^k\left|v\right|_{H^{k+1}(\tau)} \lesssim h_\tau^{k+1}r_\tau^{\delta-k-1}, \quad \forall\tau\in\mathscr{M}_h\setminus\mathscr{M}^{\widetilde{O}},$$

and that

$$\left\|\nabla(w-I_hw)\right\|_{L^2(\tau)} \lesssim h_\tau^k\left|w\right|_{H^{k+1}(\tau)} \lesssim h_\tau^{k+1}, \quad \forall\tau\in\mathscr{M}_h,$$

we have, from (3.17),

$$\begin{aligned}
\left\|\nabla(u-I_hu)\right\|_{L^2(\Omega)}^2 &\lesssim \left\|\nabla(v-I_hv)\right\|_{L^2(\Omega)}^2+\left\|\nabla(w-I_hw)\right\|_{L^2(\Omega)}^2\\
&=\sum_{\tau\in\mathscr{M}_h}\left(\left\|\nabla(v-I_hv)\right\|_{L^2(\tau)}^2+\left\|\nabla(w-I_hw)\right\|_{L^2(\tau)}^2\right)\\
&\lesssim \underline{h}^{2\delta}+\sum_{\tau\in\mathscr{M}_h\setminus\mathscr{M}^{\widetilde{O}}} h_\tau^{2k+2}r_\tau^{2\delta-2k-2}\\
&\lesssim \underline{h}^{2\delta}+\sum_{\tau\in\mathscr{M}_h\setminus\mathscr{M}^{\widetilde{O}}} r_\tau^{2k+2-2\delta}\underline{h}^{2\delta}r_\tau^{2\delta-2k-2}\\
&\lesssim \sum_{\tau\in\mathscr{M}_h}\underline{h}^{2\delta} \lesssim N\underline{h}^{2\delta} \lesssim \frac{1}{N^k}.
\end{aligned}$$

Here we have used Lemma 2.1 to derive the last inequality. This completes the proof of the lemma. $\square$

3.2. The modified PPR operator $\widehat{G}_h$

Now we introduce a definition of $\widehat{G}_h$ that satisfies conditions (i) and (ii). Given a continuous function φ, for an element $\tau \in \mathscr{M}_h$, we select $n \geq (k+2)(k+3)/2$ sampling points $z_j \in \mathscr{N}_h$, $j = 1, 2, \cdots, n$, in the element patch ω_τ containing τ, and fit a polynomial of degree $k+1$, in the least squares sense, with values of φ at those sampling points. That is, we are looking for $p_{k+1} \in \mathscr{P}_{k+1}$ such that (1.1) holds. The recovered gradient on τ is then defined as

$$\widehat{G}_h \varphi\big|_\tau = \nabla p_{k+1}\big|_\tau. \tag{3.18}$$

Let

$$p_{k+1}(x, y) = c_{0,0} + c_{1,0}x + c_{0,1}y + c_{2,0}x^2 + \cdots + c_{0,k+1}y^{k+1}.$$

Denote the n sampling points by $(x_j, y_j), j = 1, 2, \cdots, n$. Then the coefficients $c_{l,s-l}$ are determined by the following system of equations in the least squares sense:

$$c_{0,0} + \sum_{s=1}^{k+1}\sum_{l=0}^{s} c_{l,s-l} x_j^l y_j^{s-l} = \varphi(x_j, y_j), \quad j = 1, \cdots, n. \tag{3.19}$$

To reduce the effect of round-off errors, we change the above system to local coordinates:

$$\xi = \frac{x - x_1}{h_\tau}, \quad \eta = \frac{y - y_1}{h_\tau}.$$

Let

$$\begin{aligned}
&p_{k+1} = h_\tau\left(\hat{c}_{0,0} + \hat{c}_{1,0}\xi + \hat{c}_{0,1}\eta + \hat{c}_{2,0}\xi^2 + \cdots + \hat{c}_{0,k+1}\eta^{k+1}\right),\\
&\xi_j = \frac{x_j - x_1}{h_\tau}, \quad \eta_j = \frac{y_j - y_1}{h_\tau}.
\end{aligned}$$

Then (3.19) becomes

$$\hat{c}_{0,0} + \sum_{s=1}^{k+1}\sum_{l=0}^{s} \hat{c}_{l,s-l}\xi_j^l \eta_j^{s-l} = \frac{\varphi(x_j, y_j)}{h_\tau}, \quad j = 1, \cdots, n,$$

or equivalently,

$$\sum_{s=1}^{k+1}\sum_{l=0}^{s} \hat{c}_{l,s-l}\xi_j^l \eta_j^{s-l} = \frac{\varphi(x_j, y_j) - \varphi(x_1, y_1)}{h_\tau}, \quad j = 2, \cdots, n. \tag{3.20}$$

Here we have used the fact that $\xi_1 = \eta_1 = 0$. Finally, $\widehat{G}_h\varphi|_\tau$ may be calculated by using the following formula:

$$\widehat{G}_h \varphi\big|_\tau = \left(\sum_{s=1}^{k+1}\sum_{l=1}^{s} l\hat{c}_{l,s-l}\xi^{l-1}\eta^{s-l}, \sum_{s=1}^{k+1}\sum_{l=0}^{s-1}(s-l)\hat{c}_{l,s-l}\xi^l\eta^{s-l-1}\right). \tag{3.21}$$

It was proved in [18,19] that the above least squares fitting procedure has a unique solution under some mild geometric conditions. For the linear element (k=1), this condition is that: n sampling points are not on the same conic curve. Fig. 1 show possible choices of sampling points that guarantee the uniqueness of the least squares problems (3.19) (or (3.20)) for the linear and quadratic elements. It is easy to see that the above defined $\widehat{G}_h$ satisfies the condition (i), and satisfies (ii) too, if the above least squares problems are unique solvable.

4. Application to elliptic problems

Let $\Omega \subset R^2$ be a bounded polygon with boundary $\partial\Omega$. Consider the Dirichlet boundary problem: find $u \in H^1(\Omega)$ such that $u = g$ on $\partial\Omega$ and

$$A(u,v) = \int_\Omega \nabla u \cdot \nabla v = f(v), \quad \forall v \in H_0^1(\Omega), \tag{4.1}$$

where $f \in H^{-1}(\Omega)$.

Let $\mathscr{M}_h$ be a regular triangulation of the domain Ω. The finite element solution $u_h \in V_h^k$ satisfies $u_h = I_h u$ on $\partial\Omega$ and

$$A(u_h, v_h) = \int_\Omega \nabla u_h \cdot \nabla v_h = f(v_h), \quad \forall v_h \in \mathring{V}_h^k. \tag{4.2}$$

Noting that $u_h = P_h u$, under the conditions of Theorem 3.2, we have

$$\left\|\widehat{G}_h u_h - \nabla u\right\|_{L^2(\Omega)} \lesssim \frac{1+(\ln N)^{1/2}}{N^{k/2+\rho}}, \quad \rho = \min\Big(\frac{\alpha}{2}, \frac{1-\sigma}{2}\Big). \tag{4.3}$$

4.1. The a posteriori error estimate

From (4.3), it is now straightforward to prove the asymptotic exactness of error estimators based on the recovery operator $\widehat{G}_h$. The global error estimator is naturally defined by

$$\eta_h = \left\|\widehat{G}_h u_h - \nabla u_h\right\|_{L^2(\Omega)}. \tag{4.4}$$

Theorem 4.1. *Let $u_h \in V_h^k$ be the finite element approximation of u. Suppose $k = 1,2$. Assume that u satisfies* (2.1)-(2.2). *Assume that $\mathscr{M}_h$ satisfies Condition $(\alpha, \sigma, \delta/(k+1))$ with $0 < \alpha \le 1$ and $0 \le \sigma < 1$, and that $h_\tau \eqsim r_\tau^{1-\delta/(k+1)} \underline{h}^{\delta/(k+1)}$ for any $\tau \in \mathscr{M}_h$. Furthermore, assume that*

$$\frac{1}{N^{k/2}} \lesssim \left\|\nabla(u-u_h)\right\|_{L^2(\Omega)}. \tag{4.5}$$

Then

$$\left|\frac{\eta_h}{\left\|\nabla(u-u_h)\right\|_{L^2(\Omega)}} - 1\right| \lesssim \frac{1+(\ln N)^{1/2}}{N^\rho}, \quad \rho = \min\Big(\frac{\alpha}{2}, \frac{1-\sigma}{2}\Big). \tag{4.6}$$

4.2. Implementation and numerical examples

In this subsection we present some numerical examples to verify the asymptotic exactness of the error estimator η_h based on the recovery operator $\widehat{G}_h$ using quadratic finite elements.

The implementations in this paper are based on COMSOL Multiphysics and Matlab. We define the local a posteriori error estimator on element τ as,

$$\eta_\tau = \left\|\widehat{G}_h u_h - \nabla u_h\right\|_{L^2(\tau)}. \tag{4.7}$$

Then the global error estimator,

$$\eta_h = \left(\sum_{\tau\in\mathscr{M}_h} \eta_\tau^2\right)^{1/2}.$$

Now we describe the adaptive algorithm used in this section.

Algorithm 4.1. Given tolerance $\texttt{TOL} > 0$.

- Generate an initial mesh $\mathscr{M}_h$ over Ω;
- While $\eta_h > \texttt{TOL}$ do
  - Choose a set of elements $\widehat{\mathscr{M}_h} \subset \mathscr{M}_h$ such that

    $$\left(\sum_{\tau\in\widehat{\mathscr{M}_h}} \eta_\tau^2\right)^{1/2} > 0.5\left(\sum_{\tau\in\mathscr{M}_h} \eta_\tau^2\right)^{1/2},$$

    then refine the elements in $\widehat{\mathscr{M}_h}$. Update the mesh $\mathscr{M}_h$.
  - solve the discrete problem (4.2) on $\mathscr{M}_h$
  - compute error estimators on $\mathscr{M}_h$

  end while

We remark that the marking strategy, that is the method how to choose $\widehat{\mathscr{M}_h}$ for refinements, used in our algorithm, is well-known in the adaptive finite element community. Actually, it was used, e.g., in [7, 10] to design convergent finite element algorithms.

Next we test two examples. One is the cracked domain problem and another is a problem with discontinuous coefficient. Although our theoretic results do not cover the case of discontinuous coefficients, we shall shows that the asymptotic exactness of the a posteriori error estimates based on MPPR can also be observed in this case. For more numerical examples we refer to [29].

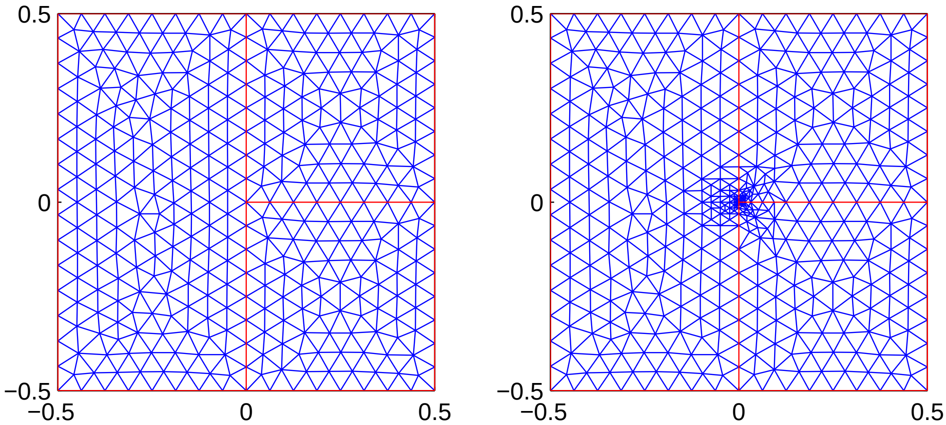

Figure 3: The initial mesh (left) and the adaptively refined mesh (right) of 991 elements after 10 adaptive iterations for the crack problem.

Example 4.1. Let $\Omega=\{(x_1,x_2):|x_1|,|x_2|<0.5\}\backslash\{(x_1,0):0\le x_1<0.5\}$ be the domain with a crack. We consider the Poisson equation

$$-\Delta u=1$$

with Dirichlet boundary condition so chosen that the true solution is $r^{1/2}\sin(\theta/2)-\frac{1}{4}r^2$ in polar coordinates.

Fig. 3 plots the initial mesh of 653 elements and the adaptively refined mesh of 991 elements after 10 adaptive iterations. Fig. 4 shows asymptotic exactness of the error estimator $\eta_h=\left\|\widehat{G}_h u_h-\nabla u_h\right\|_{L^2(\Omega)}$ for the crack problem. We see that

$$\left\|\nabla u_h-\nabla u\right\|_{L^2(\Omega)}\approx\mathcal{O}(N^{-1}),\quad \left\|\widehat{G}_h u_h-\nabla u\right\|_{L^2(\Omega)}\approx\mathcal{O}(N^{-1.15}),\tag{4.8}$$

and

$$\left\|\widehat{G}_h u_h-\nabla u_h\right\|_{L^2(\Omega)}\Big/\left\|\nabla u-\nabla u_h\right\|_{L^2(\Omega)}\approx 1+\mathcal{O}(N^{-0.3}).$$

Notice that the decay of $\left\|\nabla u_h-\nabla u\right\|_{L^2(\Omega)}$ is quasi-optimal, $\left\|\widehat{G}_h u_h-\nabla u\right\|_{L^2(\Omega)}$ is superconvergent at an order $\mathcal{O}(N^{-1.15})$, and $\eta_h/\left\|\nabla u-\nabla u_h\right\|_{L^2(\Omega)}$ approaches 1 at rate $\mathcal{O}(N^{-0.3})$ which is better than $\mathcal{O}(N^{-0.15})$ predicted by Theorem 4.1.

Next, we provide numerical verifications of Condition (α,σ,μ) and the mesh density assumption $h_\tau\eqsim r_\tau^{1-\mu}\underline{h}^\mu$ for Example 4.1. Here $\mu=1/6$ for Example 4.1. First we verify Condition (α,σ,μ). In our computations, the diameters of triangles are greater than 10^{-9}. For simplicity, we choose $\mathscr{E}_{1,h}$ to be the set of edges $e\in\mathscr{E}_h$ such that the patch Ω_e formes a 10^{-15} approximate parallelogram and $\mathscr{E}_{2,h}$ other edges in $\mathscr{E}_h$. By doing so, we actually select "exact" parallelograms for $e\in\mathscr{E}_{1,h}$, i.e., we regard e as a "good" edge if Ω_e is a parallelogram and a "bad" edge otherwise. Denote by N_{he} the number of edges $e\in\mathscr{E}_h$, and

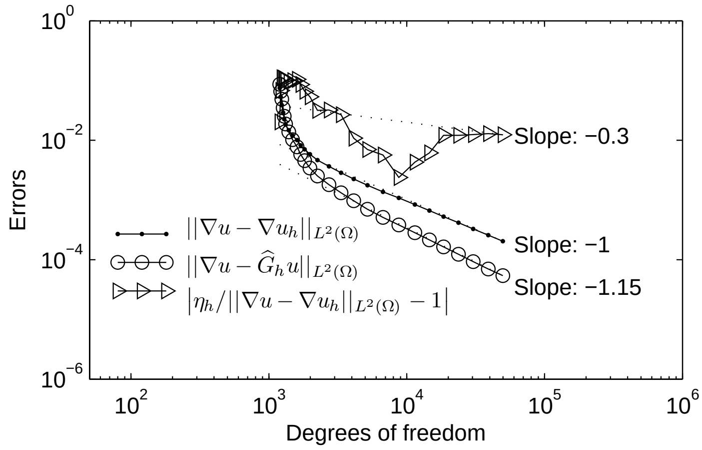

Figure 4: $\|\nabla u - \nabla u_h\|_{L^2(\Omega)}$, $\|\nabla u - \widehat{G}_h u_h\|_{L^2(\Omega)}$, and $\left|\|\widehat{G}_h u_h - \nabla u_h\|_{L^2(\Omega)} / \|\nabla u - \nabla u_h\|_{L^2(\Omega)} - 1\right|$ versus the degrees of freedom for the crack problem. Dotted lines give reference slopes.

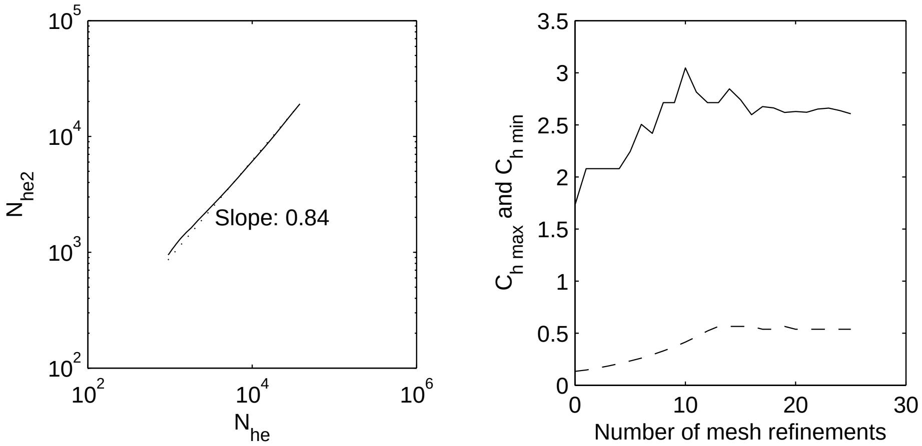

Figure 5: N_{he2} the number of "bad" edges versus N_{he} the total number of edges (left) and $C_{h\max}$ and $C_{h\min}$ versus the number of adaptive iterations (right) for Example 4.1. The dotted line gives the reference slope.

by N_{he2} the number of edges $e \in \mathscr{E}_{2,h}$. Fig. 5 (left) plots N_{he2} versus N_{he} for Example 4.1. It is shown that $N_{he2} \eqsim (N_{he})^{0.84}$. Therefore the meshes satisfy the condition $(\alpha, 0.84, \mu)$ for any $\alpha > 0$.

To verify the mesh density assumption $h_\tau \eqsim r_\tau^{1-\mu} \underline{h}^\mu$ for Example 4.1, let $C_{h\max}$ and $C_{h\min}$ be the maximum and minimum values of the set $\{h_\tau/(r_\tau^{1-\mu}\underline{h}^\mu) : \tau \in \mathscr{M}_h\}$, respectively. Here $\underline{h} = \min\{h_\tau : \tau \in \mathscr{M}_h\}$. Fig. 5 (right) depicts $C_{h\max}$ and $C_{h\min}$ versus the number of adaptive iterations for Example 4.1. The maximum and minimum values of $C_{h\max}/C_{h\min}$ are about 14.21 and about 4.60. Therefore, the mesh density assumption is satisfied.

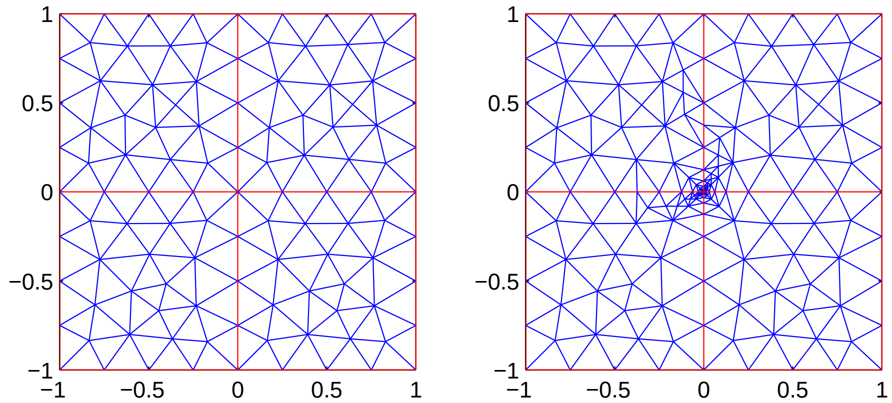

Figure 6: The initial mesh (left) and the adaptively refined mesh (right) of 334 elements after 10 adaptive iterations for Example 4.2.

Example 4.2. Let $\Omega = \{(x_1, x_2) : |x_1|, |x_2| < 1\}$ and let $\beta = 0.3$. Define $a(x,y) = (\cot(\beta\pi/4))^2$ in the first and third quadrants; $a(x,y) = 1$ in second and fourth quadrants. We consider the elliptic problem

$$-\nabla \cdot (a\nabla u) = 0$$

with Dirichlet boundary condition so chosen that the true solution is formulated in polar coordinates as

$$u = \begin{cases} -r^\beta \sin(\beta\pi/4.0)\cos(\beta(\theta - \pi/4)), & 0 \le \theta < \pi/2; \\ r^\beta \cos(\beta\pi/4.0)\sin(\beta(\theta - 3\pi/4)), & \pi/2 \le \theta < \pi; \\ r^\beta \sin(\beta\pi/4.0)\cos(\beta(\theta - 5\pi/4)), & \pi \le \theta < 3\pi/2; \\ -r^\beta \cos(\beta\pi/4.0)\sin(\beta(\theta - 7\pi/4)), & 3\pi/2 \le \theta < 2\pi. \end{cases}$$

Note that the coefficient a is discontinuous across the x-axis and the y-axis. It is clear that u does not satisfies the decomposition in (2.1) and (2.2) in the whole domain Ω but u does has such a decomposition in each of the four quadrants with $\delta = 0.3$. We shall use the weighted L^2 norm defined by $\|\cdot\|_{L^2_a} := \|a\cdot\|_{L^2}$. The local a posteriori error estimator on element τ is defined by $\eta_\tau := \left\|\widehat{G}_h u_h - \nabla u_h\right\|_{L^2_a(\tau)}$ instead of (4.7). Fig. 6 plots the initial mesh of 184 elements and the adaptively refined mesh of 334 elements after 10 adaptive iterations. Fig. 7 shows asymptotic exactness of the error estimator $\eta_h = \left\|\widehat{G}_h u_h - \nabla u_h\right\|_{L^2_a(\Omega)}$ for Example 4.2. We see that

$$\left\|\nabla u_h - \nabla u\right\|_{L^2_a(\Omega)} \approx \mathcal{O}(N^{-1}), \quad \left\|\widehat{G}_h u_h - \nabla u\right\|_{L^2_a(\Omega)} \approx \mathcal{O}(N^{-1.08}), \tag{4.9}$$

and

$$\left\|\widehat{G}_h u_h - \nabla u_h\right\|_{L^2_a(\Omega)} \Big/ \left\|\nabla u - \nabla u_h\right\|_{L^2_a(\Omega)} \approx 1 + \mathcal{O}(N^{-0.16}).$$

Notice that the decay of $\left\|\nabla u_h - \nabla u\right\|_{L^2_a(\Omega)}$ is quasi-optimal, $\left\|\widehat{G}_h u_h - \nabla u\right\|_{L^2_a(\Omega)}$ is superconvergent at an order $\mathcal{O}(N^{-1.08})$, and $\eta_h / \left\|\nabla u - \nabla u_h\right\|_{L^2_a(\Omega)}$ approaches 1 at rate $\mathcal{O}(N^{-0.16})$.

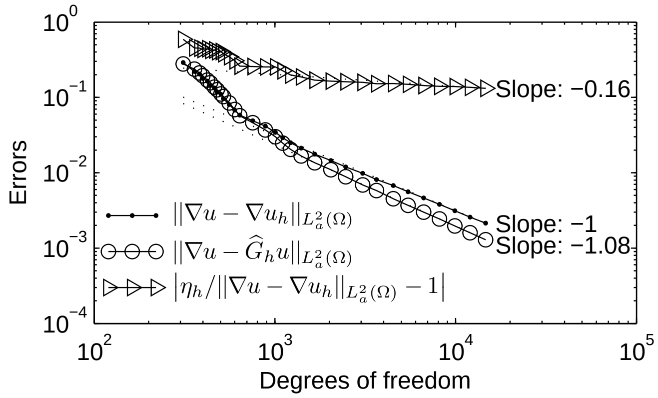

Figure 7: $\left\|\nabla u-\nabla u_h\right\|_{L^2_a(\Omega)}$, $\left\|\nabla u-\widehat{G}_h u_h\right\|_{L^2_a(\Omega)}$, and $\left|\left\|\widehat{G}_h u_h-\nabla u_h\right\|_{L^2_a(\Omega)}/\left\|\nabla u-\nabla u_h\right\|_{L^2_a(\Omega)}-1\right|$ versus the degrees of freedom for Example 4.2. Dotted lines give reference slopes.

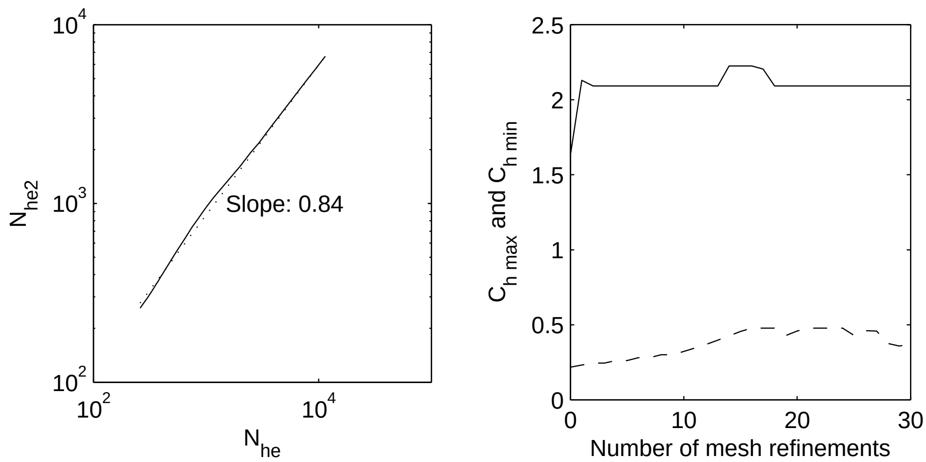

Figure 8: N_{he2} the number of "bad" edges versus N_{he} the total number of edges (left) and $C_{h\max}$ and $C_{h\min}$ versus the number of adaptive iterations (right) for Example 4.2. The dotted line gives the reference slope.

Next, we provide numerical verifications of Condition (α,σ,μ) and the mesh density assumption $h_\tau \eqsim r_\tau^{1-\mu}\underline{h}^{\mu}$ for Example 4.2. Here $\mu=0.3/3=0.1$. First we verify Condition (α,σ,μ). Fig. 8 (left) plots N_{he2} versus N_{he} for Example 4.2. It is shown that $N_{he2}\eqsim (N_{he})^{0.84}$. Therefore the meshes satisfy the condition $(\alpha,0.84,\mu)$ for any $\alpha>0$. This implies the constant $\rho=0.08$, and hence, if Theorem 3.2 holds for this example, the superconvergence order of $\left\|\widehat{G}_h u_h-\nabla u\right\|_{L^2_a(\Omega)}$ is expected to be at least $\mathcal{O}(N^{-1.08})$. This order is exactly the one that has just been observed numerically (cf. (4.9)).

On the other hand, Fig. 8 (right) depicts $C_{h\max}$ and $C_{h\min}$ versus the number of adaptive iterations for Example 4.2. The maximum and minimum values of $C_{h\max}/C_{h\min}$ are about 9.16 and about 4.37. Therefore, the mesh density assumption is satisfied.

5. Application to eigenvalue problems

The PPR technique has been used in finite element computations of eigenvalue problems on uniform meshes [20] or adaptive meshes [26] to enhance eigenvalue approximations. In this section, we shall state the corresponding results for the MPPR technique that are parallel to those from [26]. The proofs will be omitted since they are similar to those in [26].

5.1. Enhancing eigenvalue approximation by the MPPR recovered gradient

We consider a model eigenvalue problem: Find $(u,\lambda) \in H_0^1(\Omega) \times \mathbb{R}$ with $\|u\|_{L^2(\Omega)} = 1$ such that

$$a(u,v) := \int_\Omega \nabla u \cdot \nabla v = \lambda \int_\Omega uv = \lambda(u,v) \qquad \forall v \in H_0^1(\Omega), \tag{5.1}$$

where $\Omega \subset \mathbb{R}^2$ is a bounded polygonal domain with boundary $\partial\Omega$. Suppose the origin O is a vertex of Ω.

It is well known that (5.1) has a spectrum of countable infinitely many positive eigenvalues (see [13]),

$$0 < \lambda_1 \le \lambda_2 \le \cdots$$

with no finite accumulation point. Furthermore, associated eigenfunctions $u_1, u_2, \cdots$, form a complete orthonormal basis for $L_2(\Omega)$, i.e., $(u_i, u_j) = \delta_{ij}$, where δ_{ij} is the Kronecker's delta.

We want to approximate the j-th eigenvalue λ_j. Although it is possible that the eigenfunction u_j may have singularities at more than one vertices, in this paper, we consider only the case of one singular point. Suppose u_j has a singularity at the origin O and u_j satisfies (2.1)-(2.2), that is, u_j can be decomposed as a sum of a singular part and a smooth part (cf. [11]):

$$u_j = v_j + w_j \quad j = 1, 2, \cdots, \ell, \tag{5.2}$$

where

$$\left| \frac{\partial^m v_j}{\partial x^i \partial y^{m-i}} \right| \lesssim r^{\delta - m} \ \text{ and } \ \left| \frac{\partial^m w_j}{\partial x^i \partial y^{m-i}} \right| \lesssim 1, \quad m = 1, \cdots, k+2, \ \ i = 0, \cdots, m, \tag{5.3}$$

and $\delta < k+1$ is a positive constant that depends on the interior angle of the corner. Here $k = 1$ for the linear finite element and $k = 2$ for the quadratic finite element.

Given a regular triangulation $\mathscr{M}_h$ of Ω, recall that $\overset{\circ}{V}{}_h^k \subset H_0^1(\Omega)$, $k = 1, 2$, is the conforming finite element space associated with $\mathscr{M}_h$. The finite element method for (5.1) reads: Find $(u_h, \lambda_h) \in \overset{\circ}{V}{}_h^k \times \mathbb{R}$ with $\left\|u_h\right\|_{L^2(\Omega)} = 1$ such that

$$a(u_h, v_h) = \lambda_h \int_\Omega u_h v_h \qquad \forall v_h \in \overset{\circ}{V}{}_h^k. \tag{5.4}$$

The eigenvalues and eigenfunctions of the finite element approximations (5.4) are

$$\lambda_{1h} \le \lambda_{2h} \le \cdots \le \lambda_{Nh}; \quad u_{1h}, u_{2h}, \cdots, u_{Nh}; \quad (u_{ih}, u_{jh}) = \delta_{ij}.$$

The following identity is crucial for our method, see [23, Lemma 6.3] and [3, Lemma 9.1]:

$$\lambda_{jh} - \lambda_j = \left\|\nabla(u_j - u_{jh})\right\|^2_{L^2(\Omega)} - \lambda_j \left\|u_j - u_{jh}\right\|^2_{L^2(\Omega)}. \tag{5.5}$$

We have the following error estimates for $\lambda_{jh} - \lambda_j$ and $u_j - u_{jh}$ and the superconvergence between ∇u_j and $\widehat{G}_h u_{jh}$.

Theorem 5.1. *Assume that $\mathscr{M}_h$ satisfies Condition $(\alpha, \sigma, \delta/(k+1))$ with $0 < \alpha \le 1$ and $0 \le \sigma < 1$, and that $h_\tau \approx r_\tau^{1-\delta/(k+1)} \underline{h}^{\delta/(k+1)}$ for any $\tau \in \mathscr{M}_h$, $k = 1,2$. Then, there exists N_0 such that, for all $N > N_0$,*

$$0 \le \lambda_{jh} - \lambda_j \lesssim \frac{1}{N^k}, \tag{5.6}$$

$$\left\|\nabla u_j - \nabla u_{jh}\right\|_{L^2(\Omega)} \lesssim \frac{1}{N^{k/2}}, \tag{5.7}$$

$$\left\|u_j - u_{jh}\right\|_{L^2(\Omega)} \lesssim \frac{1 + (\ln N)^{1/2}}{N^{k/2+\rho}}, \tag{5.8}$$

$$\left\|\widehat{G}_h u_{jh} - \nabla u_j\right\|_{L^2(\Omega)} \lesssim \frac{1 + (\ln N)^{1/2}}{N^{k/2+\rho}}, \quad \rho = \min\Big(\frac{\alpha}{2}, \frac{1-\sigma}{2}\Big). \tag{5.9}$$

Next, we define the error estimator for the j-th eigenfunction:

$$\eta_{jh} = \left\|\widehat{G}_h u_{jh} - \nabla u_{jh}\right\|_{L^2(\Omega)}. \tag{5.10}$$

Then, from (5.5) and Theorem 5.1, we have the following asymptotic exactness of the error estimator.

Theorem 5.2. *Assume that $\mathscr{M}_h$ satisfies Condition $(\alpha, \sigma, \delta/(k+1))$ with $0 < \alpha \le 1$ and $0 \le \sigma < 1$, and that $h_\tau \approx r_\tau^{1-\delta/(k+1)} \underline{h}^{\delta/(k+1)}$ for any $\tau \in \mathscr{M}_h$, $k = 1,2$. Suppose*

$$\frac{1}{N^{k/2}} \lesssim \left\|\nabla u_j - \nabla u_{jh}\right\|_{L^2(\Omega)}. \tag{5.11}$$

Then, there exists N_0 such that, for all $N > N_0$, $j = 1, 2, \cdots, \ell$,

$$\left|1 - \frac{\eta_{jh}^2}{\left\|\nabla(u_j - u_{jh})\right\|^2_{L^2(\Omega)}}\right| \lesssim \frac{1 + (\ln N)^{1/2}}{N^\rho}, \tag{5.12}$$

$$\left|1 - \frac{\lambda_{jh} - \lambda_j}{\eta_{jh}^2}\right| \lesssim \frac{1 + \ln N}{N^\rho}, \quad \rho = \min\Big(\frac{\alpha}{2}, \frac{1-\sigma}{2}\Big). \tag{5.13}$$

The inequality (5.13) says that η_{jh}^2 is an asymptotically exact error estimator for $\lambda_{jh} - \lambda_j$ and that

$$\lambda^*_{jh} = \lambda_{jh} - \eta_{jh}^2 = \lambda_{jh} - \left\|\widehat{G}_h u_{jh} - \nabla u_{jh}\right\|^2_{L^2(\Omega)} \tag{5.14}$$

is a better approximation of λ_j than λ_{jh} under our mesh condition.

5.2. Implementation and numerical example

We define a local a posteriori error estimator on element τ as,

$$\eta_{j\tau} := \left\| \widehat{G}_h u_{jh} - \nabla u_{jh} \right\|_{L^2(\tau)},$$

and a global error estimator for λ_{jh},

$$\eta_{jh}^2 = \sum_{\tau \in \mathcal{M}_h} \eta_{j\tau}^2.$$

Now we describe the adaptive algorithm used in this section.

Algorithm 5.1. Given tolerance $\mathtt{TOL} > 0$.

- Generate an initial mesh $\mathcal{M}_h$ over Ω;
- While $\eta_{jh}^2 > \mathtt{TOL}$ do
  - Choose a set of elements $\widehat{\mathcal{M}_h} \subset \mathcal{M}_h$ such that

    $$\Big(\sum_{\tau \in \widehat{\mathcal{M}_h}} \eta_{j\tau}^2 \Big)^{1/2} > 0.7 \Big(\sum_{\tau \in \mathcal{M}_h} \eta_{j\tau}^2 \Big)^{1/2},$$

    then refine the elements in $\widehat{\mathcal{M}_h}$. Denote the new mesh by $\mathcal{M}_h$ also.
  - solve the discrete problem (5.4) on $\mathcal{M}_h$ for $\lambda_{jh}(1 \le j \le \ell)$ and let $\lambda_{jh}^* = \lambda_{jh} - \eta_{jh}^2$.
  - compute error estimators on $\mathcal{M}_h$

  end while

Note that we have suggested in the above algorithm to use $\eta_{j\tau}$, the a posteriori error estimates based on the j-th discrete eigenfunction, for mesh refinements. In the case that the first ℓ eigenvalues are all needed, we suggest to use $\eta_{1\tau}$, the a posteriori error estimates based on the 1-st discrete eigenfunction, for mesh refinements just as the algorithm proposed in [26], because the singularity of u_1 usually dominates the others.

In the following example, quadratic finite elements are used in the computation. In order to access exact eigenvalues for convergence tests, we use circular domains instead of square domains. Note that our theory covers only polygonal domains. Nevertheless, the theory can be extended to curved domains with some more involved analysis taking account the effect of curved boundaries.

Example 5.1. The eigenvalue problem (5.1) on the domain with a crack

$$\Omega = \left\{ (r, \theta) \in \mathbb{R}^2 : \ 0 < r < 1, 0 < \theta < 2\pi \right\}.$$

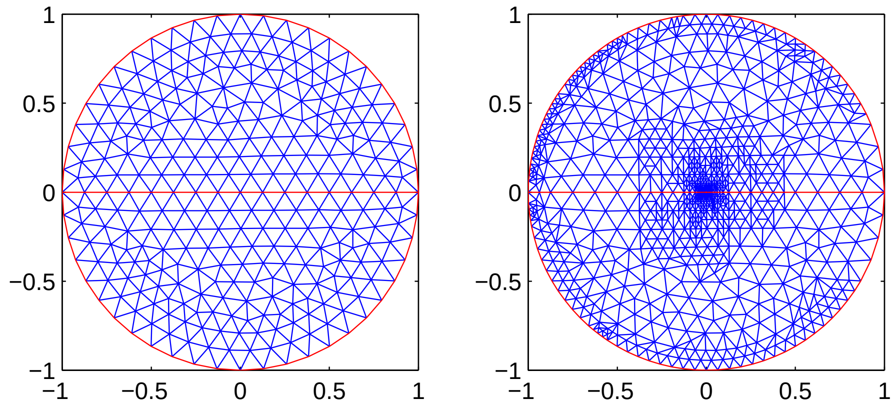

Figure 9: The initial mesh (left) and the adaptively refined mesh (right) of 1908 elements after 10 adaptive iterations for Example 5.1.

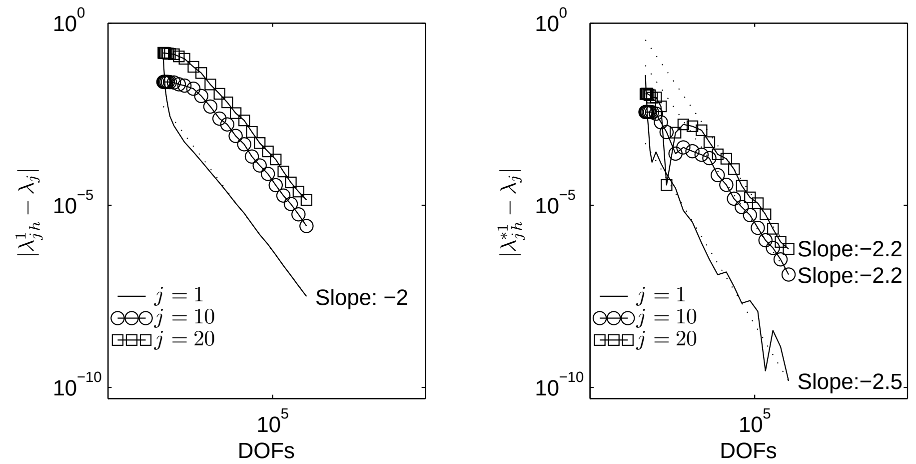

Figure 10: $\left|\lambda^1_{jh} - \lambda_j\right|$ (left) and $\left|\lambda^{*1}_{jh} - \lambda_j\right|$ (right), $j = 1, 10, 20$, versus the degrees of freedom for Example 5.1.

The eigenvalues and eigenfunctions for this example are

$$\lambda_j = \alpha_j^2, \quad u_j = v_j / \left\|v_j\right\|_{L^2(\Omega)}, \quad v_j = J_{m_j/2}(\alpha_j r)\sin(m_j\theta/2),$$

where m_j is some integer depending on j, and α_j is a zero of the Bessel function $J_{m_j/2}$. Note that $v_j = J_{m_j/2}(\alpha_j r)\sin(m_j\theta/2)$ has the same singularity as $r^{m_j/2}\sin(m_j\theta/2)$, where $m_j = 1,2,3,4,5,1,6,7,2,8,3,9,4,10,5,11,1,6,12,2$, for $j = 1,2,\cdots,20$, respectively.

It is clear that the adaptive algorithm depends on the eigenfunction used in the a posteriori error estimates. Denote by λ^k_{jh} and λ^{*k}_{jh} the j-th discrete eigenvalue and the j-th recovered eigenvalue obtained by using the a posteriori error estimates based on the k-th discrete eigenfunction, respectively. In the following, we will discuss the effect of choosing

Table 1: $\lambda_j, 1 \le j \le 20$, the errors $\left|\lambda_{jh}^1 - \lambda_j\right|$, and $\left|\lambda_{jh}^{*1} - \lambda_j\right|$ for Example 5.1 after 25 adaptive iterations.

j	λ_j	$\left\|\lambda_{jh}^1 - \lambda_j\right\|$	$\left\|\lambda_{jh}^{*1} - \lambda_j\right\|$
1	9.869604401089	3.16e-008	1.53e-010
2	14.681970642124	4.23e-008	2.87e-009
3	20.190728556427	9.83e-008	2.19e-009
4	26.374616427163	2.30e-007	1.50e-009
5	33.217461914268	4.71e-007	1.18e-008
6	39.478417604357	7.47e-007	3.02e-008
7	40.706465818200	9.39e-007	3.61e-008
8	48.831193643619	1.63e-006	7.54e-008
9	49.218456321695	1.54e-006	5.84e-008
10	57.582940903291	2.70e-006	1.26e-007
11	59.679515944109	2.54e-006	1.02e-007
12	66.954311925105	4.33e-006	2.44e-007
13	70.849998919096	4.17e-006	1.84e-007
14	76.938928333647	6.58e-006	3.67e-007
15	82.719231101493	7.06e-006	3.13e-007
16	87.531220257134	9.75e-006	5.48e-007
17	88.826439609804	6.90e-006	3.08e-007
18	95.277572544037	1.09e-005	5.08e-007
19	98.726272477249	1.44e-005	7.94e-007
20	103.499453895137	1.41e-005	6.35e-007

different discrete eigenfunctions in the a posteriori error estimates on the convergence rates of discrete eigenvalues.

First, we test our adaptive algorithm by choosing the first discrete eigenfunction for the a posteriori error estimates. Fig. 9 plots the initial mesh of 548 and the adaptively refined mesh of 1908 elements after 10 adaptive iterations. Fig. 10 shows the error between the exact eigenvalue λ_j and the eigenvalue approximation λ_{jh}^1, and the error between the exact eigenvalue λ_j and the enhanced eigenvalue approximation λ_{jh}^{*1} for Example 5.1 with $j = 1, 10, 20$, respectively. We observe that

$$\begin{aligned} &\left|\lambda_{jh}^1 - \lambda_j\right| \approx \mathcal{O}(N^{-2}), \quad j = 1, 10, 20, \\ &\left|\lambda_{1h}^{*1} - \lambda_1\right| \approx \mathcal{O}(N^{-2.5}), \quad \left|\lambda_{10h}^{*1} - \lambda_{10}\right| \approx \mathcal{O}(N^{-2.2}), \quad \left|\lambda_{20h}^{*1} - \lambda_{20}\right| \approx \mathcal{O}(N^{-2.2}). \end{aligned}$$

Note that the decays of $\left|\lambda_{jh}^1 - \lambda_j\right|$ $(j = 1, 10, 20)$ are quasi-optimal, the decays of $\left|\lambda_{jh}^{*1} - \lambda_j\right|$ $(j = 1, 10, 20)$ are faster with orders of $\mathcal{O}(N^{-2.5})$, $\mathcal{O}(N^{-2.2})$, $\mathcal{O}(N^{-2.2})$, respectively.

Table 1 demonstrates the first 20 exact eigenvalues $\lambda_j, 1 \le j \le 20$, obtained by the secant method, the error between the exact eigenvalue λ_j and the eigenvalue approximation λ_{jh}^1, and the error between the exact eigenvalue λ_j and the enhanced eigenvalue approximation λ_{jh}^{*1} for Example 5.1 after 25 adaptive iterations. We see that the enhanced eigenvalue approximations are accurate to 1 or 2 more decimal places than the original eigenvalue approximations.

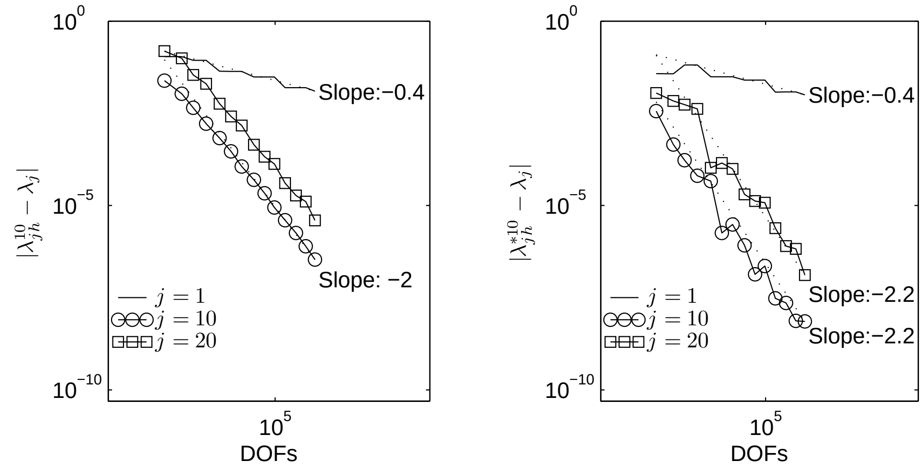

Figure 11: $\left|\lambda_{jh}^{10}-\lambda_j\right|$ (left) and $\left|\lambda_{jh}^{*10}-\lambda_j\right|$ (right), $j=1,10,20$, versus the degrees of freedom for Example 5.1.

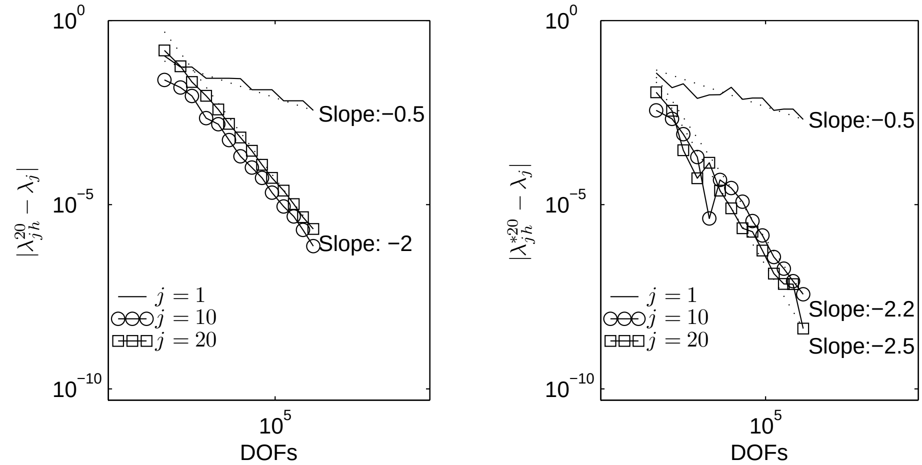

Figure 12: $\left|\lambda_{jh}^{20}-\lambda_j\right|$ (left) and $\left|\lambda_{jh}^{*20}-\lambda_j\right|$ (right), $j=1,10,20$, versus the degrees of freedom for Example 5.1.

Next we test the cases when the 10-th and 20-th eigenfunctions are used in the a posteriori error estimates, respectively. Figs. 11 and 12 plot the error $\left|\lambda_{jh}^k-\lambda_j\right|$ and $\left|\lambda_{jh}^{*k}-\lambda_j\right|$ for $j=1,10,20$, and $k=10,20$, respectively. It is shown that

$$\begin{aligned}
&\left|\lambda_{jh}^k-\lambda_j\right| \approx \mathcal{O}(N^{-2}), \quad k=10,20, \ \ j=10,20,\\
&\left|\lambda_{1h}^{10}-\lambda_1\right|, \left|\lambda_{1h}^{*10}-\lambda_1\right| \approx \mathcal{O}(N^{-0.4}), \quad \left|\lambda_{1h}^{20}-\lambda_1\right|, \left|\lambda_{1h}^{*20}-\lambda_1\right| \approx \mathcal{O}(N^{-0.5}),\\
&\left|\lambda_{10h}^{*10}-\lambda_{10}\right|, \left|\lambda_{20h}^{*10}-\lambda_{20}\right|, \left|\lambda_{10h}^{*20}-\lambda_{10}\right| \approx \mathcal{O}(N^{-2.2}), \quad \left|\lambda_{20h}^{*20}-\lambda_{20}\right| \approx \mathcal{O}(N^{-2.5}).
\end{aligned}$$

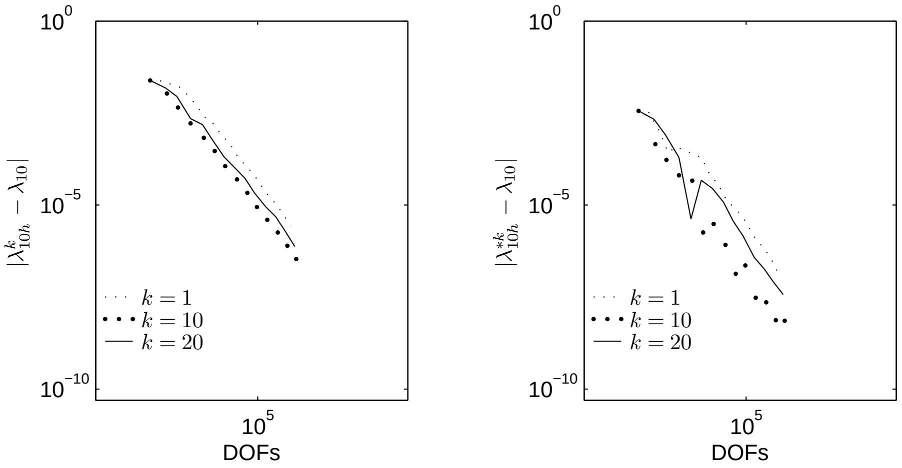

Figure 13: $\left|\lambda_{10h}^k - \lambda_{10}\right|$ (left) and $\left|\lambda_{10h}^{*k} - \lambda_{10}\right|$ (right), $k = 1, 10, 20$, versus the degrees of freedom for Example 5.1.

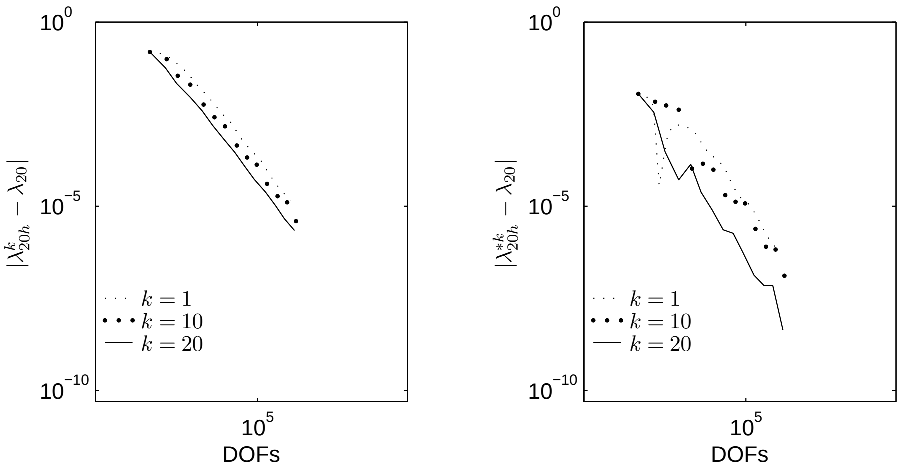

Figure 14: $\left|\lambda_{20h}^k - \lambda_{20}\right|$ (left) and $\left|\lambda_{20h}^{*k} - \lambda_{20}\right|$ (right), $k = 1, 10, 20$, versus the degrees of freedom for Example 5.1.

Note that the decays of $\left|\lambda_{jh}^k - \lambda_j\right|$ $(k = 10, 20,\ j = 10, 20)$ are quasi-optimal, while the decays of $\left|\lambda_{1h}^k - \lambda_1\right|$ $(k = 10, 20)$ are not, and that the errors $\left|\lambda_{jh}^{*k} - \lambda_j\right|$ $(k = 10, 20,\ j = 10, 20)$ are superconvergent, while the errors $\left|\lambda_{1h}^{*k} - \lambda_1\right|$ $(k = 10, 20)$ are not.

On the other hand, it is obvious that the decay of $\left|\lambda_{1h}^1 - \lambda_1\right|$ is much faster than the decays of $\left|\lambda_{1h}^k - \lambda_1\right|$ $(k = 10, 20)$, respectively. So is the decay of $\left|\lambda_{1h}^{*1} - \lambda_1\right|$. To compare the approximations to the 10-th and 20-th eigenvalues, we illustrate $\left|\lambda_{jh}^k - \lambda_j\right|$ and $\left|\lambda_{jh}^{*k} - \lambda_j\right|$ $(k = 1, 10, 20)$ versus the degrees of freedom for $j = 10$ and $j = 20$ in Figs. 13 and 14, respectively. We observe that $\left|\lambda_{jh}^j - \lambda_j\right|$ converges faster than $\left|\lambda_{jh}^k - \lambda_j\right|$ $(k \neq j)$, so is $\left|\lambda_{jh}^{*j} - \lambda_j\right|$. We suggest to use the a posteriori error estimates based on the j-th discrete eigenfunctions if only the j-th eigenvalue is cared, and to use the a posteriori error estimates based on the 1-st discrete eigenfunctions if the first ℓ eigenvalues are all needed.

Acknowledgments The work of the author was partially supported by the national basic research program of China under grant 2005CB321701 and by the program for the new century outstanding talents in universities of China.

References

[1] M. Ainsworth and J.T. Oden. *A Posteriori Error Estimation in Finite Element Analysis*. Wiley Interscience, New York, 2000.

[2] W. Babgerth and R. Rannacher. *Adaptive Finite Element Methods for Differential Equations*. Birkhäser, Basel, 2003.

[3] I. Babuška and J.E. Osborn. *Handbook of Numerical Analysis Vol.II, Finite Element Methods (Part I)*, chapter Eigenvalue problems., pages 641–792. Elsevier, 1991.

[4] I. Babuška and T. Strouboulis. *The Finite Element Method and its Reliability*. Oxford University Press, London, 2001.

[5] R.E. Bank and J. Xu. Asymptotically exact a posteriori error estimators, part i: Grid with superconvergence. *SIAM J. Numer. Anal.*, 41:2294–2312, 2003.

[6] S.C. Brenner and L.R. Scott. *The Mathematical Theory of Finite Element Methods*. Springer-Verlag, Berlin, 2002.

[7] J. M. Cascon, C. Kreuzer, R.H. Nochetto, and K.G. Siebert. Quasi-optimal convergence rate for an adaptive finite element method. *SIAM J. Numer. Anal.*, 46(5):2524–2550, 2008.

[8] L. Chen and J. Xu. Topics on adaptive finite element methods. Preprint, 2006.

[9] L. Chen and J. Xu. *Adaptive Computations: Theory and Algorithms*, chapter Topics on adaptive finite element methods. Number 6 in Mathematics Monograph Series. Science Publisher, 2007.

[10] W. Dörfler. A convergent adaptive algorithm for poisson's equation. *SIAM J. Numer. Anal.*, 33:1106–1124, 1996.

[11] P. Grisvard. *Singularities in Boundary Value Problems*. Springer-Verlag, Berlin, 1992.

[12] B.-O. Heimsund and X. Tai. *Recent Advances in Adaptive Computation*, chapter A two-mesh superconvergence method for mesh adaptivity, pages 225–238. Number 383 in Contemp. Math. American Mathematical Society, 2005.

[13] J.R. Kuttler and V.G. Sigillito. Eigenvalues of the laplacian in two dimensions. *SIAM Review*, 26(2):163–193, 1984.

[14] Marek I. Lakhany, A. M. and J. R. Whiteman. Superconvergence results on mildly structured triangulations. *Comput. Methods Appl. Mech. Engrg.*, 189:1–75, 2000.

[15] B. Li and Z. Zhang. Analysis of a class of superconvergence patch recovery techniques for linear and bilinear finite elements. *Numer. Methods Partial Differential Equations*, 15:151–167, 1999.

[16] K. Mekchay and R. H. Nochetto. Adaptive finite element methods for general second order linear elliptic pdes. *SIAM J. Numer. Anal.*, 43(5):1803–1827, 2005.

[17] P. Morin, R. H. Nochetto and K. G. Siebert. Convergence of adaptive finite element methods. *SIAM Review*, 44(4):631–658, 2002.

[18] A. Naga and Z. Zhang. A posteriori error estimates based on polynomial preserving recovery. *SIAM J. Numer. Anal.*, 42(2):1780–1800, 2004.

[19] A. Naga and Z. Zhang. The polynomial-preserving recovery for higher order finite element methods in 2d and 3d. *Discrete and Continuous Dynamical Systems - Series B*, 45(3):769–798, 2005.

[20] A. Naga, Z. Zhang, and A. Zhou. Enhancing eigenvalue approximation by gradient recovery. *SIAM J. Sci. Comput.*, 28(4):1289–1300, 2006.

[21] L. Shen and A. Zhou. A defect correction scheme for finite element eigenvalues with application to quantum chemistry. *SIAM J. Sci. Comput.*, 28(1):321–338, 2006.

[22] R. Stevenson. Optimality of a standard adaptive finite element method. *Foundations of Computational Mathematics*, 7:245–269, 2007.

[23] Strang and G.J. Fix. *An Analysis of the Finite Element Method*. Printice-Hall, Enlewood Cliffs, New Jersey, 1973.

[24] R. Verfürth. *A Posteriori Error Estimation and Adaptive Mesh Refinement Techniques*. Teubner Skripten zur Numerik, B.G. Teubner, Stuttpart, 1995.

[25] H. Wu and Z. Zhang. Can we have superconvergent gradient recovery under adaptive meshes? *SIAM J. Numer. Anal.*, 45(4):1701–1722, 2007.

[26] H. Wu and Z. Zhang. Enhancing eigenvalue approximation by gradient recovery on adaptive meshes. *IMA J. Numer. Anal.*, 28(4):1–15, 2008.

[27] J. Xu and Z. Zhang. Analysis of recovery type a posteriori error estimators for mildly structured grids. *Math. Comp.*, 73:1139–1152, 2003.

[28] N. Yan and A. Zhou. Gradient recovery type a posteriori error estimates for finite element approximations on irregular meshes. *Comput. Methods Appl. Mech. Engrg.*, 190:4289–4299, 2001.

[29] C. Ye. A modified polynomial preserving gradient recovery technique in finite element methods. Master's thesis, Nanjing University, 2009.

[30] Z. Zhang. Polynomial preserving gradient recovery and a posteriori estimate for bilinear element on irregular quadrilaterals. *Internat. J. Numer. Anal. Model.*, 1:1–24, 2004.

[31] Z. Zhang. Polynomial preserving recovery for anisotropic and irregular grids. *Journal of Computational Mathematics*, 22(2):331–340, 2004.

[32] Z. Zhang. *Adaptive Computations: Theory and Algorithms*, chapter Recovery techniques in finite element methods. Number 6 in Mathematics Monograph Series. Science Publisher, 2007.

[33] Z. Zhang and A. Naga. A new finite element gradient recovery method: Superconvergence property. *SIAM J. Sci. Comput.*, 26(4):1192–1213, 2005.

[34] O.C. Zienkiewicz and J.Z. Zhu. A simple error estimator and adaptive procedure for practical engineering analysis. *Internat. J. Numer. Methods Engrg.*, 24:337–357, 1987.

[35] O.C. Zienkiewicz and J.Z. Zhu. The superconvergence patch recovery and a posteriori error estimates, part 1: The recovery technique. *Internat. J. Numer. Methods Engrg.*, 33:1131–1364, 1992.

[36] O.C. Zienkiewicz and J.Z. Zhu. The superconvergence patch recovery and a posteriori error estimates, part 2: Error estimates and adaptivity. *Internat. J. Numer. Methods Engrg.*, 33:1365–1382, 1992.

[37] Taylor R.L. Zienkiewicz, O.C. and J.Z. Zhu. *The Finite Element Method, 6th ed.* McGraw-Hill, London, 2005.